

# Micro-macro Analysis of the Notch Tip Radius and Loading Rate Dependences of the Dynamic Crack Initiation Toughness during a High Transient Dynamic crack Growth Experiment

D. Grégoire<sup>1</sup>, H. Maigre<sup>1</sup>, R. Estevez<sup>2</sup>, A. Combescure<sup>1</sup>

<sup>1</sup>*LaMCoS, INSA-LYON, CNRS UMR5259, F69621 Villeurbanne, France;*

<sup>2</sup>*MATEIS, INSA-LYON, CNRS UMR5510, F69621 Villeurbanne, France*

*E-mail: david.gregoire@insa-lyon.fr*

## 1. Introduction

The risks due to crack propagation under dynamic loading are still difficult to estimate. Unlike quasi-static cases, where the loading and crack position can be easily established, in dynamic impact cases, loading conditions, propagation parameter variations and exact crack positions are difficult to control. The determination of relevant constitutive crack propagation laws from dynamic crack propagation experiments is thus a challenging operation. Consequently, the first step for assessing dynamic crack propagation laws is the development of numerical simulation tools. Some numerical tools are now able to represent dynamic crack growth but these numerical results have to be compared with experimental results to ensure that the numerical laws introduced are physically consistent. In a previous work [1], crack tip position histories have been determined by standard optical tools. The test rig was a split Hopkinson pressure bar (SHPB) and the specimen geometry was chosen in order to provide direct conversion between impacting compressive waves and tensile waves in the vicinity of a machined notch. Since the material used (PMMA) was transparent, the crack tip position history was obtained by using standard optical tools (four cameras providing one picture per camera) and by carrying out the same tests, repetitively and reproducibly. Three different phases were observed: two propagation phases were separated by a crack arrest phase. Using an eXtended Finite Element Method (X-FEM), numerical simulations were performed and both the crack path and the crack position histories fitted the experimental results. Failure in glassy polymers has been extensively investigated for PMMA, which is well documented [2, 3, 4]. The toughness under mode I loading increases with loading rate and its value is also notch sensitive. Therefore, the criterion adopted in the foregoing X-FEM analysis with a set of parameters for the onset of crack advance, its dynamic propagation, arrest and conditions for re-propagation appears to approximate the rate-dependent process underlying failure. However this kind of comparison allowed the validation of a dynamic crack growth criterion but only in a unique case of loading. The previous process leads to a large experiments number for obtaining different crack tip position histories corresponding to different loading rate and the loading rate influence on the transient propagation phases as arrest and restart cannot be represented accurately if several experiments are needed to obtain a crack tip position history. Therefore the experimental setup has been improved by replacing the cameras with a

Zimmer extensometer. It leads to a very accurate crack tip localization and provides the whole propagating crack tip position history for each test performed as shown in [5] in pure mode I conditions with several consecutive crack arrest phases. This paper focuses on the use of the same experimental setup in order to study the influence of the loading rate on the transient propagation phases as arrest and restart in mixed-mode conditions.

## 2. Experimental setup

The test rig is a split Hopkinson Pressure Bar (SHPB or Kolsky bars) test developed by Kolsky [6] and primarily used for the measurement of a material dynamic behavior. The test specimen is made of polymethylmethacrylate (PMMA), a transparent brittle material. The bars are chosen made of nylon, a quite similar material, in order to guarantee both a good wave transmission on their interfaces with the specimen and an elastic strain gage response. Details on the experimental setup are presented in [1] and [5]. There is no standard for dynamic impact fracture tests. Therefore a simple, but distinctive, geometry designed is chosen to obtain transient propagation phases as crack arrest and restart. A rectangular specimen with a circular hole is used to provide both the direct wave conversion from compressive waves into tensile waves and the crack arrest zone. A radial initial notch is machined at the border of the hole in order to initiate the crack in mixed-mode conditions as shown Fig. (1).

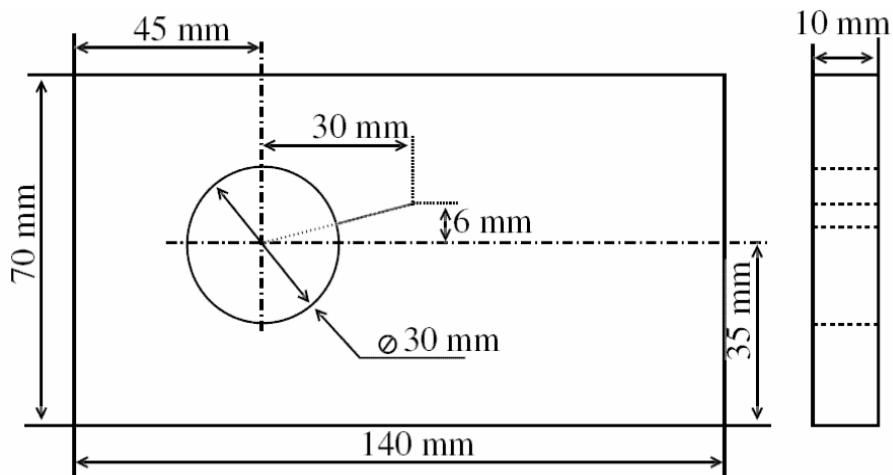


*Fig 1. Specimen geometry*

The use of SHPB is attractive because it provides both an accurate measurement of the applied loading and the global response of the test specimen during the transient experiment. Wave dispersion and geometry effects are taken into account in the shifting of the mechanical data to the specimen-bar interfaces as in [7]. The experimental test rig includes the striker bar, the input bar, the output bar and the specimen between the bars; 2 strain gages connected to their amplifiers; 2

optical displacement sensors Zimmer 115 and Zimmer 116 with different measuring ranges (see Table 1).

Zimmer	115	116
Measurement range [mm]	100	20
Measurement width [mm]	5	1
Uncertainty [mm]	$\pm 0.2$	$\pm 0.04$

Table 1. Characteristics of the optical displacement sensors.

Since the signal delivered by the extensometer takes into account the specimen solid body displacement in addition to the crack tip displacement, a correction is processed in order to obtain the real crack growth. Four different tests are performed at different impact velocities. The experimental conditions are described in Table 2 and the crack tip positions histories for each Zimmer extensometers in Fig. (2).

Experiment	Test 1	Test2	Test 3	Test 4
Striker velocity [m/s]	8.35	10.3	11.2	12.6

Table 2. Experimental conditions.

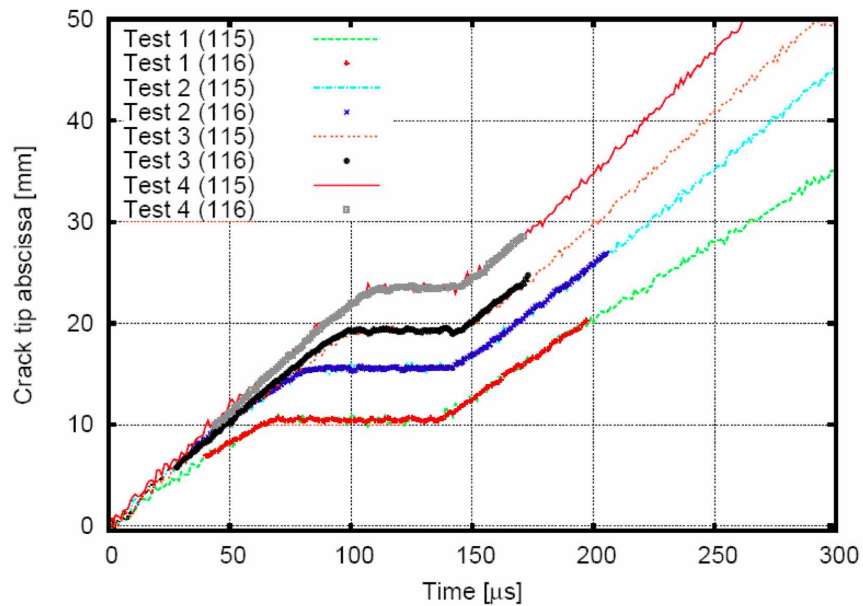


Fig 2. Experimental crack tip position histories for the four tests (Zimmer 115 and Zimmer 116).

Fig. (2) reveals that this method based on optical displacement sensor measurement provides an accurate crack tip localization. For each test, the signals delivered by each extensometer agree and the highly transient propagation phases

such as arrest and restart are easily distinguishable. Thus, the influence of the loading rate on the crack arrest and restart phases can be noticed. The lower is the striker velocity, the lower is the horizontal crack tip velocity, the earlier occurs the crack arrest phase and the longer lasts the crack arrest phase.

### 3. Numerical comparison

The eXtended Finite Element Method is chosen for the simulation because the cracks are not described explicitly by the mesh. It allows the mixed-mode dynamic propagation laws validation because the crack path is considered a priori unknown. This method consists in using an enrichment to the classical finite element approximation in order to capture the discontinuity and the singularity of the strain fields at the crack tip. It was first developed for quasi-static analysis in [8] and then used for dynamic crack propagation in [1] in the light of [9]. The numerical simulation are carried out using the input velocity collected from the experiments as a boundary condition at the input bar interface and an impedance condition is used to model the contact between the output bar and the specimen. Even if the PMMA is known to be viscoelastic, a linear elastic behavior is assumed with a dynamic elastic modulus fitted with the velocity of the elastic waves measured during the experiment. An example of comparison between experimental and numerical results is presented in Fig. (3) in order to show how this numerical tool can be used to validate crack propagation laws. The dynamic crack propagation laws assumed are quite simple, chosen according to the global macroscopic concept of stress intensity factors [10] extended to elastodynamics within the framework of [11, 12].

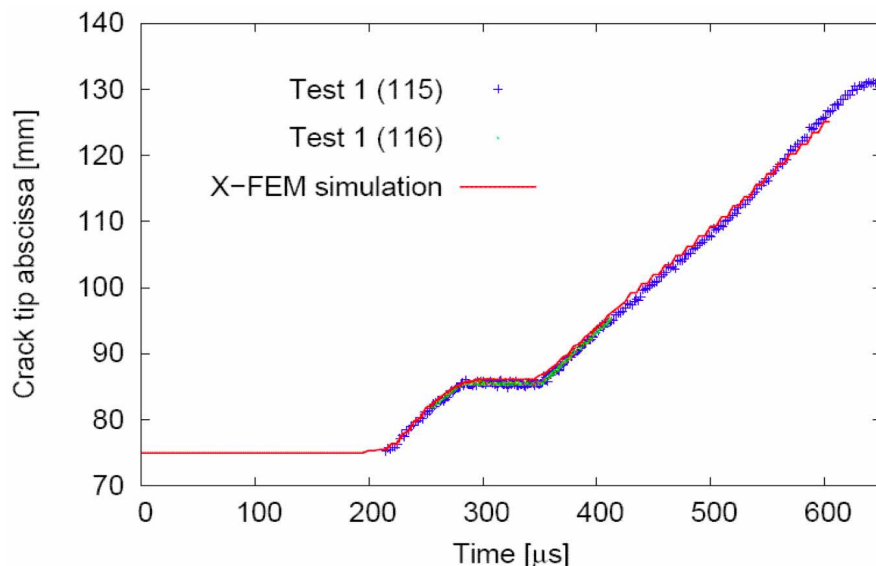


Fig 3. Comparison of crack tip position histories for the test 1.

The fracture phenomenon is assumed to be governed by the intensity of the hoop stress near the crack tip as in [13] and a dynamic crack growth criterion is chosen to take the crack growth process into account as in [14] (the formulation can be found in [1]). On the Fig. (3), a good matching of the numerical and experimental results is obtained but the criteria have to be involved in order to well-represent the loading rate dependencies noticed in Fig. (2).

#### 4. Micro-macro analysis

In this part, we present estimates of the rate and notch dependence of the energy release rate and related toughness based on a micromechanical analysis of the failure by crazing, with all the parameters involved in the description being identified for the same material as that used to the dynamic fracture analysis. At the crack tip region and under mode I, failure in amorphous polymers potentially involves strain localization by shear yielding and fracture by crazing. We briefly recall the description of crazing and the related thermomechanical analysis. Indeed, temperature effects are expected as soon as the loading rate exceeds  $\dot{K}_I > 100\text{MPa}\sqrt{\text{m/s}}$ , with the viscoplastic contribution due to the crazing process being the dominant heat source [15]. We use cohesive zone description used [16, 17] and calibrated for crazing at low rates [18]. Upon craze initiation, craze thickening proceeds by the growth of fibrils that bridge the craze surfaces. Based on Kramer's description [2], the transformation of the bulk material into a fibril take place within a thin active plastic zone of some nanometers in between the fibrils-bulk interface. Based on this observation, Tijssens et al. [16] postulated the following craze opening rate

$$\dot{\Delta}_n^c = \dot{\Delta}_0 \exp\left\{\frac{-A}{T}(\sigma^c - \sigma_n)\right\}$$

where  $\dot{\Delta}_0$ ,  $A$  and  $\sigma^c$  are material parameters. The term  $A$  accounts for the temperature dependence,  $\sigma^c$  is the athermal stress for craze thickening,  $\sigma_n$  the traction along the craze surface, while the pre-exponential  $\dot{\Delta}_0$  has the dimension of a velocity. Thus, the thickening rate of the craze is temperature and time dependent. Once crazing has initiated, the thickening process continues until the cumulated  $\Delta_n^c = \int \dot{\Delta}_n^c dt$  reaches a critical thickness  $\Delta^{ct}$ , a material parameter that primarily depends on the temperature and on the molecular weight (Döll in [2,3]). The governing equations are taken from Estevez et al. [15] with the mechanical and thermal parts being solved in a staggered way. Heat from craze fibrillation is incorporated through a heat flux across the craze surfaces into the bulk. The magnitude of the heat flux across the cohesive surface is  $\sigma_n \dot{\Delta}_n^c$ . In order to account for some energy stored by the web of craze fibrils during the craze thickening, only a fraction  $\beta^{CZ} \sigma_n \dot{\Delta}_n^c$  with  $\beta^{CZ}$  taken as 0.5, similarly to the value found for the bulk when temperature from the bulk viscoplasticity are arising as in compression. The temperature increase related to the craze thickening can

promote an increase in the craze critical opening (Döll in [2, 3]) observed to be twice that at room temperature near the glass transition  $T_g$  for PMMA.

The bulk as well as the cohesive zone parameters for crazing realistically describe PMMA as they are obtained from detailed calibration experiments [18] and thermal properties. At high rates, we observed that viscoplasticity from the bulk is inhibited by the crazing process which acts as a mechanical fuses and prevent material from yielding. Therefore, crazing is the only possible heat source. The related temperature variations remain confined along the craze-crack surfaces over a length which appears of the order of the craze thickness. Similarly to Estevez et al. [15], we analyse mode I fracture within a plane strain small scale yielding configuration in which the bulk viscoplastic response is accounted for. Crazing is considered along the crack symmetry plane where it most probably takes place. The thermomechanical analysis is borrowed to [15] to which the reader is referred for further details.

In Fig. (4), we report the measures of the variations of the energy release rate with loading rate [19]. These correspond to samples in which a sharp notch has been created by tapping a fresh razor blade at the tip of a machined pre-notch. The fracture tests consist in fast three points bending tests with a prescribed displacement rate ranging in 1-5m/s [19].

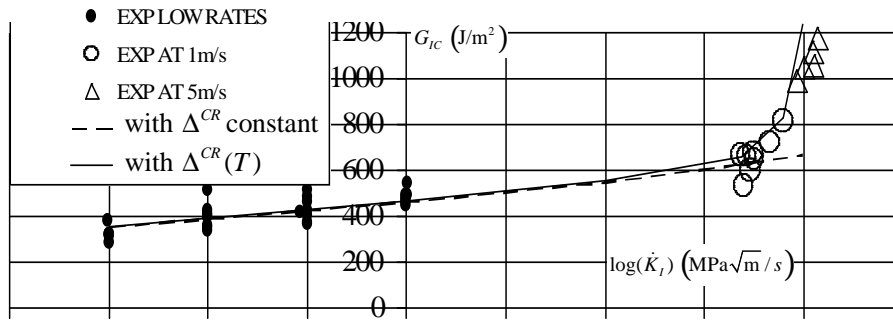


Fig 4. Variations of the energy release rate with loading rate from low to high rates on samples with a sharp notch. The low rates ( $\dot{K}_I \leq 1 \text{MPa}\sqrt{\text{m/s}}$ ) and the high rates  $\dot{K}_I > 1 \times 10^3 \text{MPa}\sqrt{\text{m/s}}$  measures are taken from [19, 21], the prediction of the failure based on a viscoplastic cohesive zone with a temperature dependence of the craze critical opening capture the experimental data over 7 decades in loading rates.

In Fig. (4), it is observed that the energy release rate exhibits a marked increase around  $\dot{K}_I \approx 1 \times 10^4 \text{MPa}\sqrt{\text{m/s}}$  and a time to failure about 0.1ms. These experimental data are then used to assess the calibration performed at low rates, presented in [18]. As shown in [19], the predictions based on the calibration of

Saad et al. [18] is valid up to a time to failure about 1ms ( $\dot{K}_I \leq 2 \times 10^3 \text{MPa}\sqrt{\text{m/s}}$ ) but fails in capturing the increase of the energy release rate for higher loading rates. The prediction with the marked rise in  $G_{IC}$  with  $\dot{K}_I$  is obtained by accounting for a temperature dependent craze critical opening  $\Delta^{CR}(T)$ , of which variation runs from  $\Delta^{CR}(T_{AMBIENT}) = 3\mu\text{m}$  to  $\Delta^{CR}(T_g) = 6\mu\text{m}$ . The best agreement between the predictions and the measures of the energy release rate with loading rate is obtained by considering a parabolic variation of  $\Delta^{CR}(T)$  with the temperature, as reported in Fig.(4).

The above calibration, extended for high rates is now used to investigate the influence of the notch size and loading rate effects of the fracture properties (toughness and related energy release rate). The corresponding variations are reported in Fig. (5). We have reported the results for a sharp crack prepared by tapping together with other predictions with different crack configurations. These correspond to various initial notch radii of 0.25mm and 0.1mm that are closed to those machined in the dynamic fracture experiments. We have also considered notch radii of 0.25mm and 0.1mm with an initial defect along the crack symmetry plane of which length is taken of 25 microns in order to estimate the influence of an initial defect that results in a small crack along the notch, that could originate from the machining. We have reported the variations corresponding to the results for the sharp crack of Fig. (4). In all cases, the toughness at the onset of crack propagation is seen to increase non linearly with the loading rate. For a given loading rate, the toughness increases with the crack radius with the lowest value for the tapping's configuration, then that of 0.1mm and the highest value for a blunt notch of 0.25mm. It is worth noting that introducing an initial defect of 25 $\mu\text{m}$  induces a noticeable drop in the level of the toughness. For the blunt notch of 0.1mm, the account for the initial defect results in a variation of the toughness comparable to that for the tapping. For the notch of 0.25mm with a defect, the toughness is reduced down to an intermediate level between that of the perfect radius of 0.1mm and the sharp crack prepared by tapping.

The predictions of the toughness and related dependence with the notch radius and loading rate are noticeably influenced by the quality of the notch machined and possible presence of an initial defect. Therefore, a direct comparison with the dynamic fracture tests is not straightforward as the quality of the notch contour is difficult to assess. The variations of the toughness with initial notch radius and loading rate provide valuable trends for the calibration of the parameters governing the crack propagation in the dynamic fracture X-FEM simulations. Also, one has to keep in mind that the prescribed stress state in the local approach under pure mode I differs from those prescribed during the dynamic tests with a noticeable mixed mode I/II arising. This second aspect is a limitation in the present study that could be overcome by performing a multiscale analysis in which the local description would be embedded in a more macroscopic one. However, these first results are thought to pave the route towards that direction.

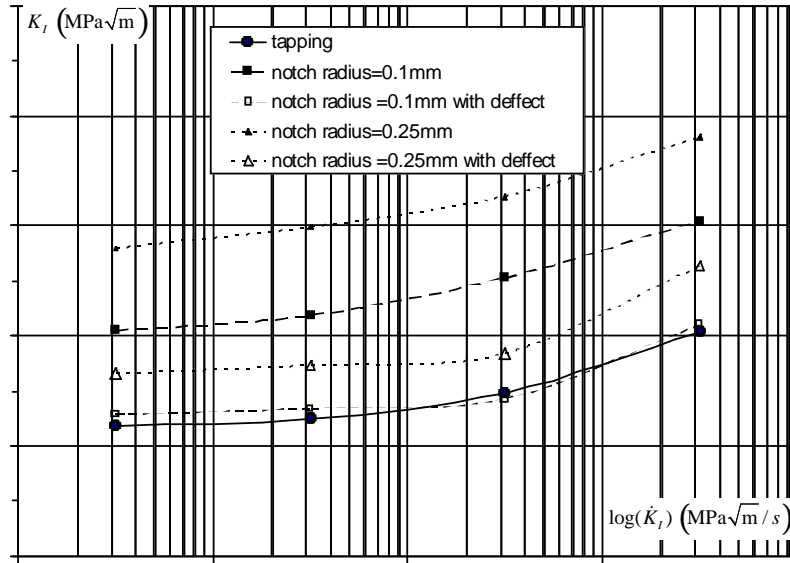


Fig 5. Variation of the toughness with loading rate at the onset of crack propagation under mode I for a sharp crack –tapping–, blunt notches with radius of 0.25mm and 0.1mm, and blunt notches with an initial defect along the crack symmetry plane of 25 microns long.

## Conclusion

This work shows that a good combination of well-controlled experiments and refined X-FEM simulations enables one to explain the history of brittle dynamic crack propagation and arrest using simple ingredients. The new experimental setup presented allows the assessment and the validation of new dynamic crack growth criteria by studying the highly transient propagation phases such as crack growth, crack arrest and crack restart. To take into account the dependency of those criteria with the initial condition of the crack propagation (notch radius) and the loading rate we have performed a micro-macro scale analysis using micromechanical analysis of the failure by crazing. The predictions give the good trends compare to the experiments and further work has to be done to include this analysis in a macro criterion.

## Acknowledgement

This work was sponsored by an ANR/CNRS grant DynRupt (JC05\_45254) and by a BQR grant from INSA-Lyon.

## References

- [1] D. Grégoire, H. Maigre, J. Réthoré, A. Combescure: *Int. J. Solids Struct.*, 44, (2007) 6517-6534
- [2] Kausch HH (Ed) *Adv. Polym. Sci.,Crazing*, Springer Heidelberg-Berlin, 1983, pp. 52-53
- [3] Kausch HH (Ed) *Adv. Polym. Sci.*, Springer, Heidelberg-Berlin 1990, pp. 91-92
- [4] Williams JG, *Fracture Mechanics of Polymers*, Ellis Horwood, New York, 1984
- [5] D. Grégoire, H. Maigre, F. Morestin : *Eur. J. Comput. Mech.* (2008), accepted
- [6] H. Kolsky: *P. Phys. Soc.*, B62, (1949) 676-700
- [7] H. Zhao, G. Gary: *J. Mech. Phys. Solids*, 43(8), (1995) 1335-1348
- [8] N. Moës, J. Dolbow, T. Belytschko: *Int. J. Numer. Meth. Eng.*, 46, (1999) 131-150
- [9] J. Réthoré, A. Gravouil, A. Combescure: *Int. J. Numer. Meth. Eng.*, 63, (2005) 631-659
- [10] G. Irwin: *J. Appl. Mech.*, 24(3), 361-364
- [11] H. D. Bui: *Mécanique de la rupture fragile*, Masson, Paris, 1978
- [12] L. B. Freund: *Dynamic Fracture Mechanics*, Cambridge University Press, Cambridge, 1990
- [13] H. Maigre, D. Rittel: *Int. J. Solids Struct.*, 30(23), (1993) 3233-3244
- [14] M. Kanninen, C. H. Popelar: *Advanced Fracture Mechanics*, Oxford University Press, 1985.
- [15] Estevez R., Basu S., Van der Giessen E., *Int. J. Fact.*, 132 (2005) 249-273
- [16] Tijssens MGA, Van der Giessen E, Sluys LJ, *Mech Mat* , 32 (2000)19
- [17] Estevez R, Tijssens MGA, Van der Giessen E, *J Mech Phys Sol* 48 (2000) 2585-2617
- [18] Saad-Gouider N., Estevez R., Olagnon C., Séguéla R., *Engng. Fract .Mech.* 73 (2006) 2503-2522.
- [19] Estevez R., Saad-Gouider N., Olagnon C., Sautereau H., (2008), *Int. J. Fract*, in preparation